Published in IET Optoelectronics
Received on 21st June 2012
Revised on 19th November 2012
Accepted on 9th December 2012
doi: 10.1049/iet-opt.2012.0047

ISSN 1751-8768

Modelling of free space optical link for ground-to-train communications using a Gaussian source

Rupak Paudel, Zabih Ghassemlooy, Hoa Le-Minh, Sujan Rajbhandari

Optical Communications Research Group, NCRLab, Faculty of Engineering and Environment, Northumbria University, Newcastle upon Tyne, UK
E-mail: rupak.paudel@northumbria.ac.uk

Abstract: The demand for access to broadband data services in high-speed trains is increasing as more people are travelling to and from work, which is not met by the existing radio frequency technology. Therefore an alternative technology known as free space optics (FSO) could be readily adopted that could overcome the bandwidth bottleneck problem. The study presents a mathematical model of an FSO link for ground-to-train communications link and analyses the system performance in terms of the signal-to-noise ratio and the bit error rate (BER). The authors show that the simulated BER is in good agreement with the predicted results for bit rates up to 50 Mbps. The link budget analysis for the proposed system is also presented showing a link margin of 17.75 dB.

1 Introduction

Free-space optical (FSO) communications is an alternative wireless access technology to the existing radio frequency (RF) wireless systems. FSO also known as the optical wireless communications have multiple advantages that can complement the existing RF links such as huge unregulated spectrum, immunity to electromagnetic interference, high security since optical beams do not penetrate opaque objects and frequency reuse resulting in a high capacity per unit volume [1–5]. The FSO system is the preferred option, where there is limitation or restriction in the use of RF-based systems in application including hospitals, airplane, military where RF interferes with monitoring equipment. The FSO technology can be utilised in both indoor and outdoor environment capable of supporting very high data rates up to gigabit per second. Various works [3, 6, 7] have reported indoor FSO communications with data rates beyond 1 Gb/s. For outdoor systems, 100 Gb/s per channel link is reported in [8], whereas 1.28 Tb/s FSO link (32×40 Gb/s) is reported in [1] using the dense wavelength division multiplexing. FSO supports a number of modulations, forward error correction coding schemes and protocols for a variety of applications, including voice and multimedia services. FSO is also designed to support a large number of users, with multiple connections per terminal, each with its own quality of service requirement. In indoor FSO systems mobility offered is not as advanced as in the RF technology. The FSO technology is relatively young but mature and its widespread deployment will in parts depend on (i) the cost of devices as compared with the RF technology, and (ii) how the RF dominated industry will see FSO not as a threat but a complementary technology to RF in areas where there is a need for a high-speed link.

Owing to the exponential growth of handheld devices such as smart-phones or tablets, there is a growing demand for high-speed internet connections in trains, ships, buses etc. The existing infrastructure based on the RF technology such as Wi-Fi/WiMAX used in trains are capable of delivering, theoretically, peak data rates up to 54/75 Mbps, where in real scenario this could be lower than 10 Mbps at the best of times [9]. This of course is inadequate and does not meet the customers' expectations. The bandwidth bottleneck [10] could be improved by increasing the carrier frequency, thus by adopting the millimetre wave technology beyond the 60–80 GHz band. In the future, the offered internet facilities are expected to be falling short of the increasing demand for high-quality multimedia type services in train. One possible and viable solution to address the demand for higher data rates is the FSO. A ground-to-train communications system using the FSO technology is proposed in [11], where a tracking control algorithm is used to establish a stable communication link between the mobile unit and the ground. In [12], an FSO system with a faster handover mechanism (124 ms) is proposed to achieve a data rate in excess of 500 Mbps in high-speed trains. Although, practical-based data are reported by Hiruta *et al.* [11] and Haruyama *et al.* 12], a detailed mathematical modelling of the FSO ground-to-train communication link, which is essential for system modelling and performance analysis has not been addressed. In our previous work [13], we have reported a mathematical model for the FSO ground-to-train system using a Lambertian source. In such systems, laser sources are the preferred option for higher power requirements and longer coverage length and can be modelled as Gaussian. This paper outlines a mathematical model for the FSO ground-to-train communications link and introduces a new expression for the received optical

power based on the proposed geometrical model. The proposed system would be a complementary technology to RF–based schemes providing higher data rates for the end users. In this proposed system, intensity modulation with direct detection, which is the most popular method in FSO, is incorporated because of its simplicity and low cost. The rest of the paper is organised as follows: Section 2 discusses the proposed system along with the mathematical model, Section 3 presents system design, Section 4 presents results along with discussion and Section 5 concludes the paper.

2 System modelling

A typical ground-to-train FSO communication link is shown in Fig. 1. The link consists of optical transceivers (Tx/Rx) positioned on the roof of the train and base stations (BSs) positioned alongside the train track. Each BS emits a narrow width optical beam fully covering the entire train. BSs are only active when the train is within its transmission range and the optical footprint, otherwise they are in the off mode to save energy. Exchange of information from BS to the service provider will take place via the fibre-optic backbone network, which is normally laid down along the rail tack as in UK.

The proposed geometrical model of the downlink communications for an over-ground train for a straight track is depicted in Fig. 2. Usually for a straight track, the maximum span between the power overhead lines (gantries) is 75 m [14], which is used as the spacing between the BSs in this analysis. Of course the BS separation can be extended to few hundred metres for a longer track. In this scenario, one could either increase the transmit power at the BS within the eye-safe limit, which is further explained in Section 3.3 or move to a longer wavelengths of 1300 nm and 1550 nm where eye safety is not a major issue compared with lower wavelengths.

In this section, we will model the available received optical power distributed along the track length L, see Fig. 2. The BS is positioned a metre away from the track, and is adjustable. Let the half angle divergence be $\theta_{1/2}$ (i.e. $\theta = 2\theta_{1/2}$). The BS transmitter (A), which is at the same height as the optical Tx/Rx (i.e. ~ 4 m above the ground level), could be tilted by an angle $\theta_{1/2} + \delta$ represented by γ along the horizontal plane so that it points towards the optical Rx. $\overline{CD}$ (d_2) is the horizontal separation distance between BS and the shortest coverage point C, which can be varied in order to estimate the transmitter's beam divergence angle θ. $\overline{AD}$ (d_1) is fixed at 1 m (BS separation from the track), δ is the coverage angle at the longest point B and β is the coverage angle at the shortest point C. Using a simple geometry, $\theta = \beta - \delta$ and for $\triangle$ACD and $\triangle$ABD, respectively, we have $\tan\beta = (d_1/d_2)$ and $\tan\delta = (d_1/(d_2 + L))$. The estimated transmitter beam divergence angle can be written as

$$\theta = \tan^{-1} \frac{d_1 L}{d_1^2 + d_2 L + d_2^2} \tag{1}$$

Hence, based on the position of the BS and the effective coverage length, the beam divergence angle can be approximated. The optical beam radius of a Gaussian beam

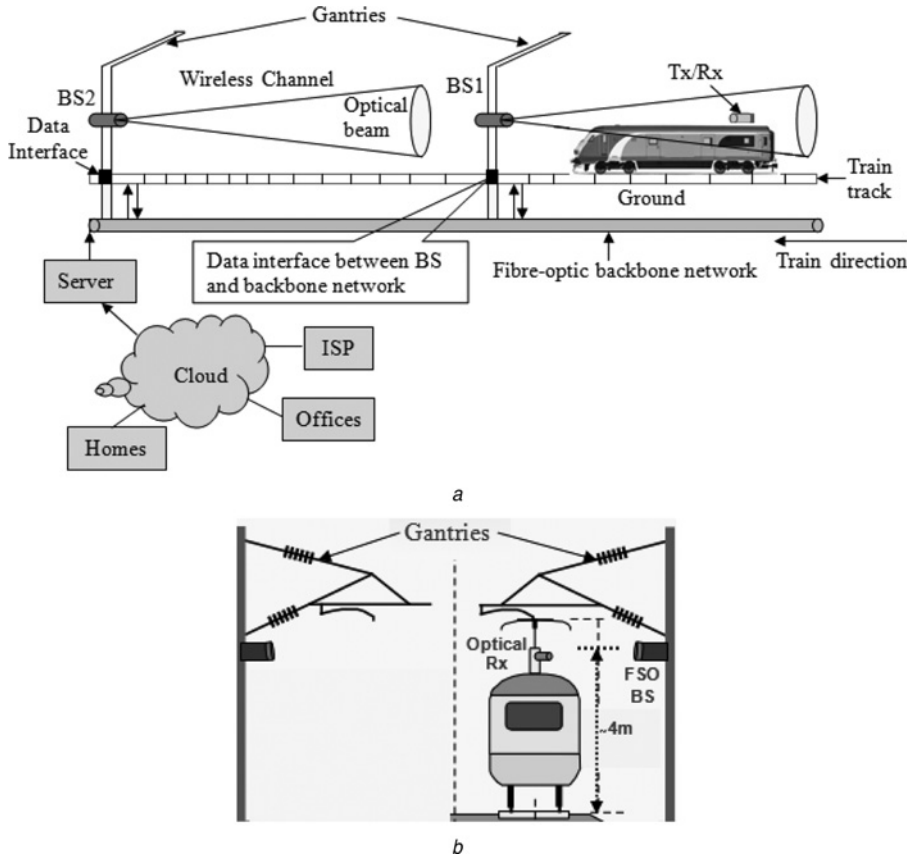

Fig. 1 *Typical ground-to-train FSO communication link*

a Typical ground-to-train communications system and
b Front view of the proposed system

doi: 10.1049/iet-opt.2012.0047

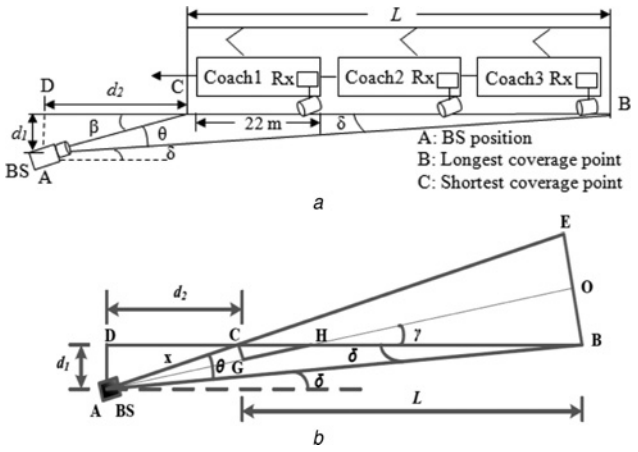

Fig. 2 *Proposed geometrical model of the downlink communications for an over-ground train for a straight track*

a Proposed system geometrical modelling
b System geometry

is given as [15]

$$w = w_0 \left[1 + \left(\frac{\lambda z}{\pi w_0^2}\right)^2\right]^{(1/2)} \tag{2}$$

where w_0 is the beam waist of the laser source at the transmitter, z is the axis of propagation and λ is the operating wavelength of the optical source.

In Fig. 2, let $\overline{AC}$ be denoted by x ($= \sqrt{d_1^2 + d_2^2}$). The $\angle$OHB (see Fig. 2*b*)) can be written as $(\theta_{1/2} + \delta)$ and represented by γ. The following analysis is performed in order to derive a general equation for the power received along the track. Here, the length along the axis of propagation, $\overline{AO}$ (z) would be related to length CB, which is the effective coverage length L so that the power along L could be determined. From Fig. 2*b*, $z = AH + HO$ and the length AH can be written as $AG + GH$. Similarly, length HO can be written as $HO = (L - CH)\cos\gamma$. Hence z can be given as $z = AG + GH + (L - CH)\cos\gamma$. Using basic geometry, z can be written as

$$z = L\cos\gamma + x\cos\theta_{1/2} \tag{3}$$

Rewriting the beam radius from (2) in terms of the effective coverage length along the track using (3) as

$$w = w_0 \left[1 + \left(\frac{\lambda\left(L\cos\gamma + x\cos\theta_{1/2}\right)}{\pi w_0^2}\right)^2\right]^{(1/2)} \tag{4}$$

In ΔOHB, denoting OB as the offset r from the axis AO at the point B, we obtain $r = (L - CH)\sin\gamma$. Hence, the radial offset from the axis of propagation AHO orthogonal to the axis can be written as

$$r = \left(L\sin\gamma - x\sin\theta_{1/2}\right) \tag{5}$$

The received power at the receiver along the z-axis for a Gaussian beam is given by [15]

$$P_{rx} = \frac{2P_{tx}A_{coll}}{\pi w^2} e^{-\left(2r^2/w^2\right)} \tag{6}$$

where P_{tx} is the total transmit power from BS and A_{coll} is the collection area at the receiver. Using (4)–(6), P_{tx} along the track $\overline{CB}$, when the BS is positioned at a distance d_1 from the track based on the Gaussian beam profile, is given as (see (7))

Once the average optical transmitter power, the collection area of the receiver, beam divergence, the tilting angle of the receiver at the longest coverage point, the BS position and the effective coverage length are determined, the received power can be evaluated using (7). The angular parameters for the model and the system model parameters used for the simulation are given in Tables 1 and 2, respectively.

Table 1 Angular parameters

Symbol	Parameters	Calculated, deg.
θ	beam divergence	3.20
ψ_c	receiver FOV	5.15
δ	coverage angle at B	0.65
β	coverage angle at C	3.85
γ	Tx/Rx tilting angle	2.25

Table 2 System model parameters

Symbol	Parameters	Value
λ	operating wavelength	850 nm
d_1	vertical position of BS	1 m
d_2	horizontal BS position	15 m
A_{det}	photodetector area	7 mm^2
P_{tx}	BS optical transmit power	15 mW
S_r	receiver sensitivity	– 36 dBm @ 10 Mbps
R	responsivity	0.59 A/W
R_{coll}	radius of the optical concentrator	25 mm
f	focal length of the lens	50 mm
n	refractive index of the telescope	1.5
L	coverage length	75 m
D	source diameter	5 mm
P_n	noise power	10 μW

3 System design

This section describes the optical wireless link for the proposed system, which consists of an optical transmitter and a receiver and a wireless communications channel. Also

$$P_{rx} = \frac{2P_{tx}A_{coll}\cos\gamma}{\pi w_0^2\left[1 + \left(\lambda\left(\left(L\cos\gamma + x\cos\theta_{(1/2)}\right)/\pi w_0^2\right)\right)^2\right]} \exp\left(-\frac{2\left(L\sin\gamma - x\sin\theta_{(1/2)}\right)^2}{w_0^2\left[1 + \left(\left(\left(\lambda\left(L\cos\gamma + x\cos\theta_{(1/2)}\right)\right)/\pi w_0^2\right)\right)^2\right]}\right) \tag{7}$$

the eye safety analysis is discussed for the average transmitter power and the link budget analysis is performed for the system.

3.1 Transmitter

The transmitter comprises of a laser source and a laser driver, which can be modulated using the most common modulation format non-return-to-zero (NRZ) on–off keying (OOK). The transmitter parameters such as the beam divergence and the average transmit power for the system is estimated based on the proposed geometrical model. The beam divergence is estimated from the positions of d_1 and d_2 and L as given by (1). The transmit power at the BS can be derived from (6) by replacing the received power with the receiver sensitivity and for $L = 75$ m.

3.2 Receiver

The receiver positioned on the roof of the train will be tilted at an angle γ. This is also the angle made by the propagation axis with the train track so that the field-of-view (FOV) of the receiver at both the longest and shortest points B and C, respectively, will be within the beam divergence of the transmitter. The receiver incorporates an optical concentrator, a photodiode and receiver electronics. The concentrator collects and focuses the incoming light onto the photodiode, whereas the receiver electronics is used to recover the signal. The concentrator gain at the receiver can be evaluated as [16]

$$g(\psi) = \begin{cases} \dfrac{n^2}{\sin^2 \psi_c}, & 0 \le \psi \le \psi_c \\ 0, & \text{elsewhere} \end{cases} \tag{8}$$

where n is the refractive index of an optical concentrator and ψ_c is the half-angle FOV of the receiver after the lens. The FOV of the receiver using the optical concentrator is given by [17]

$$A_{\text{coll}} \sin^2 \psi_c = n^2 A_{\text{det}} \tag{9}$$

where A_{coll} is the effective light collection area of the receiver and A_{det} is the area of the photodetector. The proposed system parameters are tabulated in Table 1. The noise source at the detector is the combination of the shot noise, the thermal noise [18] and the background noise [19]. The typical value for the background radiation used is 10 μW [20, 21]. The total noise variance can be written as

$$\sigma^2_{\text{total}} = \sigma^2_{\text{sh}} + \sigma^2_{\text{th}} + \sigma^2_{\text{bg}} \tag{10}$$

where σ^2_{sh} σ^2_{th} and σ^2_{bg} has the variance because of shot noise, thermal noise and the background noise, respectively. The total noise present at the detector can be modelled as the additive white Gaussian noise (AWGN). The signal-to-noise ratio (SNR) at the receiver is hence given by [16]

$$\text{SNR} = \frac{(RP_{\text{rx}})^2}{\sigma^2_{\text{total}}} \tag{11}$$

The BER for OOK–NRZ is then evaluated as

$$\text{BER} = Q\left(\sqrt{\text{SNR}}\right) \tag{12}$$

where

$$Q(x) = \frac{1}{2\pi} \int_x^{\infty} \mathrm{e}^{(-y^2/(2))}\, \mathrm{d}y$$

3.3 Eye safety

In order for the system to operate in public places, the utilised optical source should conform to the international eye safety standards [22]. The acceptable emission limit (AEL) is determined by the angular subtense angle and the operating wavelength. The angular subtense of the apparent source should be calculated in order to classify the laser source used based on Fig. 3, which depends on the source diameter as

$$\alpha = 2 \tan^{-1} \frac{D}{2r_{\text{measure}}} \tag{13}$$

where r_{measure} (= 100 mm) is the measuring distance and D is the source diameter. D is assumed to be 5 mm, therefore the source can be classified as an extended source since the angular subtense can be calculated as 50 mrad as given by (13), which lies in between α_{min} and α_{max} of 1.5 and 100 mrad, respectively. With $P_{\text{tx}} = 15$ mW, which is below the AEL limit of 20 mW for an exposure time of 100 s for extended source when the operating wavelength is 850 nm, the system proposed conforms to the eye safety standards. If higher power transmission is required, we can move to higher wavelengths around 1300 nm, where the AEL limit increases by a factor of 20 as compared with that of 850 nm. In this work, 850 nm wavelength is adopted as this is the most commonly used window for optical communications where the components available are the cheapest [23].

3.4 Link budget analysis

The link budget analysis is performed in order to evaluate the system link margin after taking into account losses associated with the system. The losses considered are the atmospheric loss because of weather conditions, the geometrical loss L_{geom}, the pointing loss L_{pt}, the transmitter loss L_{tx} and the receiver loss L_{rx}. The attenuation of a laser beam in the atmosphere is described by Beer's law [24]. The link visibility is derived from the fog attenuation using the Kim model to reflect the attenuation in dB/km as [2]

$$L_{\text{fog}}\ (\text{dB/km}) = \frac{17}{V[\text{km}]} \left(\frac{\lambda}{550\ \text{nm}}\right)^{-q} > 0 \tag{14}$$

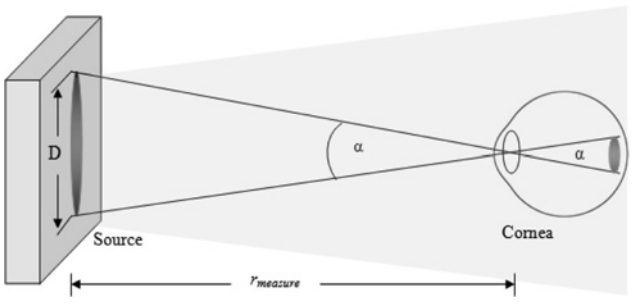

Fig. 3 *Angular subtense measurement*

doi: 10.1049/iet-opt.2012.0047

where V is the meteorological visibility in km, λ is the wavelength in nm and q is the size distribution of scattering particles and is given by [25]

$$q = \begin{cases} 1.6 & V > 50\,\text{km} \\ 1.3 & 6\ \text{km} < V < 50\,\text{km} \\ 0.16\,\text{V} + 34 & 1\,\text{km} < V < 6\,\text{km} \\ V - 0.5 & 0.5\,\text{km} < V < 1\,\text{km} \\ 0 & V < 0.5\,\text{km} \end{cases} \quad (15)$$

Using (14) for a moderate fog, that is, visibility of 500 m, fog attenuation is calculated as 34 dB/km. The other loss in the system is because of the spreading of the transmitted beam as it propagates through the atmosphere known as the geometrical loss. Geometrical loss can be approximated by the following expression for a uniform transmitter power distribution [26]

$$L_{\text{geom}} = 10\ \log\left[\frac{d_{\text{r}}}{(d_{\text{t}} + \theta L)}\right]^2 \quad (16)$$

where d_{r} is the receiver aperture diameter, and d_{t} is the transmitter aperture diameter. Typical transmitter/receiver loss is considered to be 3 dB. The link budget equation can be written as

$$M = P_{\text{tx}} + S_{\text{r}} + G_{\text{rx}} - L_{\text{fog}} - L_{\text{geom}} - L_{\text{tx}} - L_{\text{rx}} - L_{\text{pt}} \quad (17)$$

where M is the link margin of the system, S_{r} is the receiver sensitivity of the photodetector, and G_{rx} is the gain of the optical concentrator. Table 3 shows the link budget analysis for this system with a link margin of nearly 18 dB after considering all different losses in the system.

3.5 Train aerodynamics and turbulence effect

The train moving at a high speed creates aerodynamic forces around the train. These forces are influenced by three factors namely, train speed, distance from the train and the train geometry [27]. At low train speeds, there is a significant velocity variation around the train height with high turbulence intensity. The turbulence intensity is low at high train speeds with more uniform velocity profile [28]. The moving train creates a boundary layer along the train length resulting in the airflow in the direction of the train and a wake behind it. As shown in Fig. 4, although the movement of the train creates pressure peaks at front and back ends of the train, there is a uniform pressure along the length of the train carriage [27]. Train moving at high speed induces wind in its surrounding [27]. At a speed of about 200 km/h, it would generate wind speeds of about 15 m/s [29]. According to Deng *et al.* [30], the link performance improves with the wind speed. To illustrate this, we use the method adopted in [30], where the mean <SNR> as a function of SNR with no turbulence SNR_0 is given by [31]

$$\text{SNR} = \frac{\text{SNR}_0}{\sqrt{1 + \sigma_{\text{I}}^2(\text{SNR}_0)^2}} \quad (18)$$

where σ_{I}^2 is the scintillation index for various wind speed for a Gaussian beam as given by [30] (see (19))

where $\alpha = 11/3$ for Kolmogorov spectrum, $\tilde{\sigma}_B^2$ denotes the longitudinal component of the scintillation index, $\tilde{\sigma}_{\text{R}}^2$ is a non-Kolmogorov Rytov variance for plane wave, $f_X(\alpha, \bar{\Theta})$ and $f_Y(\alpha)$are large-scale and small-scale parameters, $\bar{\Theta}$ is curvature parameter, Λ is Fresnel ratio, σ_{pe} denotes an effective pointing error, W_{LT}^2 is long-term spot size caused by large-scale-induced beam wander, W is the free-space beam spot radius and r is the radial distance from the optical axis. Fig. 5 shows the system performance as a function of the wind speed based on (18) and (19) where <SNR> (gain) increases for increasing wind speed. Positioning the transceiver in the middle part of the train roof, where the pressure is almost constant and as a result the refractive index is almost constant would make the FSO link less susceptible to the turbulence effect. Although when the train is stationary, the scintillation index variation because of the pressure and temperature would be high, but for a train moving at a constant speed the turbulence effect can be ignored because of the constant pressure and temperature along the length of the train. The link margin of 17.75 dB would ensure that the system is functioning at all conditions.

Table 3 Link budget

Parameters	Value
transmitter	
• power	11.80 dBm
• losses (L_{tx})	– 3 dB
• pointing loss (L_{pt})	– 5 dB
channel losses($L_{\text{fog}} + L_{\text{geom}}$)	– 43 dB
receiver losses (L_{rx})	– 3 dB
receiver telescope gain	24 dB
receiver sensitivity	– 36 dBm
link margin – for weather conditions	17.75 dB

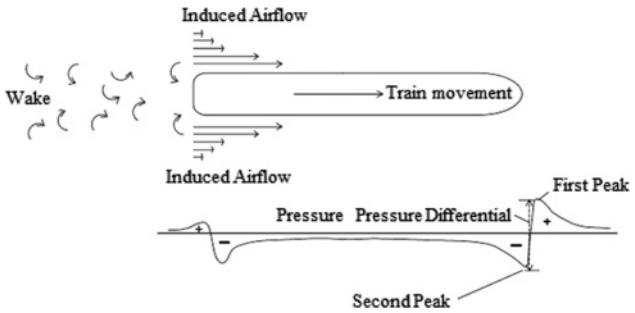

Fig. 4 *Air flow around the train (courtesy of [27])*

$$\sigma_{\text{I}}^2 = \exp\left(\frac{0.49\tilde{\sigma}_B^2}{\left(1 + f_X(\alpha, \bar{\Theta})\tilde{\sigma}_{\text{R}}^{(4/(\alpha-2))}\right)^{3-(\alpha/2)}} + \frac{0.51\tilde{\sigma}_B^2}{\left(1 + f_Y(\alpha)\tilde{\sigma}_B^{(4/(\alpha-2))}\right)^{(\alpha/2)-1}}\right) - 1 + 4.42\tilde{\sigma}_{\text{R}}^2\Lambda_e^{(\alpha/2)-1}\left(\frac{\sigma_{\text{pe}}}{W_{\text{LT}}}\right)^2 + 4.42\tilde{\sigma}_{\text{R}}^2\Lambda_e^{(\alpha/2)-1}\left(\frac{r - \sigma_{\text{pe}}}{W_{\text{LT}}}\right)^2, 3 < \alpha < 4, 0 \le \sigma_{\text{R}}^2 \le \infty, \sigma_{\text{pe}} \le r \le W \quad (19)$$

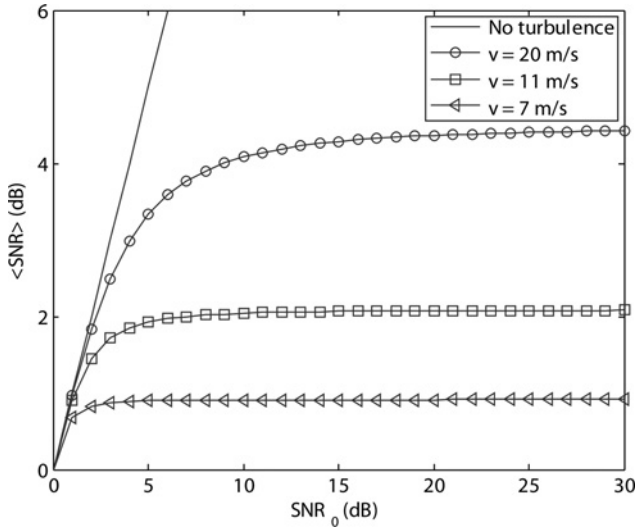

Fig. 5 *Mean SNR as a function of SNR with no turbulence for various wind speeds (adapted from [30])*

4 Results and discussion

The numerical analysis of the proposed system is performed using MATLAB®. The communications channel for this terrestrial FSO link is assumed to be AWGN channel in our simulation. To estimate the appropriate beam divergence θ, the horizontal BS position d_2 is varied from 5 to 25 m and the beam divergence values for a range of d_2 are shown in Fig. 6. For d_2 below 15 m, because of the wide beam divergence of over 5° and 10° at d_2 of 10 and 5 m, respectively, the required transmitted power is over 20 and 50 mW, respectively, as most of the transmit power is wasted. This is due to a large amount of power, which is outside the train-BS communications area as the beam profile is circular. When $d_2 > 15$ m, although the required transmitted power is low (<15 mW) but the received power fades away quickly since the BS position is further away from the shortest coverage point C. The power profile for different values of d_2 is plotted and compared in Fig. 7 based on (7), which suggests that the power profile appears to be more uniform for d_2 values over 15 m. Since, the desired BS separation distance from the shortest coverage point C along the track is small, the horizontal BS position value is chosen to be 15 m. Using (1), the beam divergence for the track coverage length of 75 m, fixing d_1 at 1 m and $d_2 = 15$ m, would be 3.20° as is evident from Fig. 6.

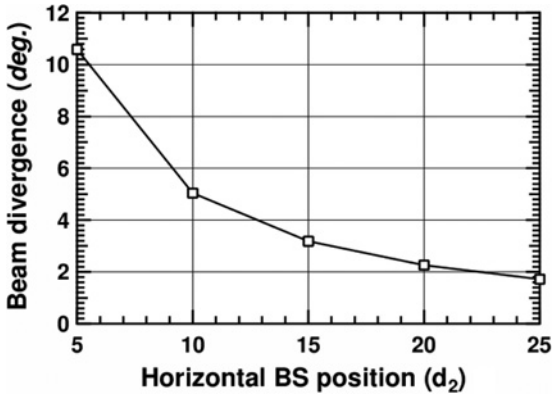

Fig. 6 *Beam divergence for varying d_2*

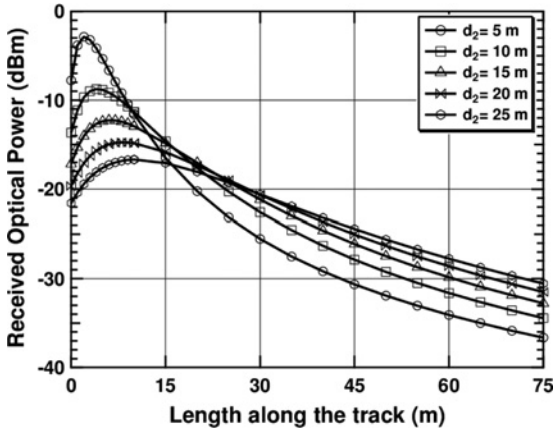

Fig. 7 *Power profile variation for varying d_2*

Assuming a typical *Rx* sensitivity of −36 dBm at 10 Mbps, and a radius of receiver optics of 25 mm, the required transmit power at the BS is taken to be 11.8 dB (15 mW) as in Table 3. The receiver FOV is estimated based on the size of the receiver optics as given in (9). Based on the parameters considered, the optimum receiver semi-FOV for a 7 mm^2 photodetector would be 5.15° (half angle). For this link, a margin of ∼18 dB is used, which is evident from the link budget analysis. The transmitter power could be increased to the AEL limit as discussed above to ensure 100% link availability.

The SNR along the track for various bit rates are shown in Fig. 8. The simulation is performed up to a data rate of 100 Mbps because of the limitation in the bandwidth (50 MHz) of the measured laser impulse response, which is adopted for simulation. As can be seen, to achieve a SNR of 13.6 dB the effective coverage length for the data rate of 10 Mbps is 75 m. However, the observed SNR within the link margin offers an additional SNR of 10 dB, that is, 23.6 dB at 10 Mbps. Increasing the bit rate to 100 Mbps does not affect the theoretical coverage length of 75 m. The SNR drops from 23.6 dB at 10 Mbps to 13.6 dB at 100 Mbps since the noise bandwidth increases at higher bit rates for a constant transmit power.

The BER performance of the ground-to-train system is evaluated based on the angular parameters in Table 1 and system model parameters in Table 2. The BER curve along the train track for various bit rates is plotted in Figs. 9*a* and *b* for beam divergence angles of 3.2° and 4°, respectively. The plot for a 4° beam angle (commercially available

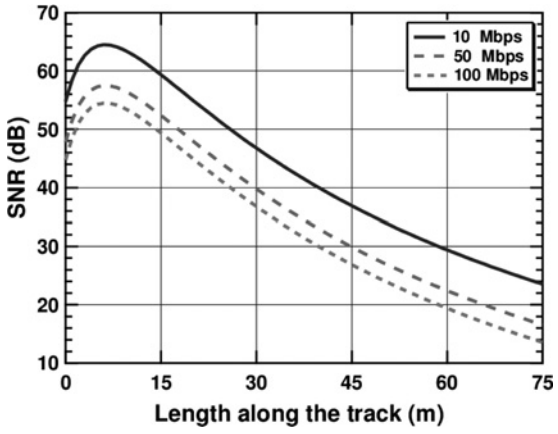

Fig. 8 *SNR variation along the track length CB*

doi: 10.1049/iet-opt.2012.0047

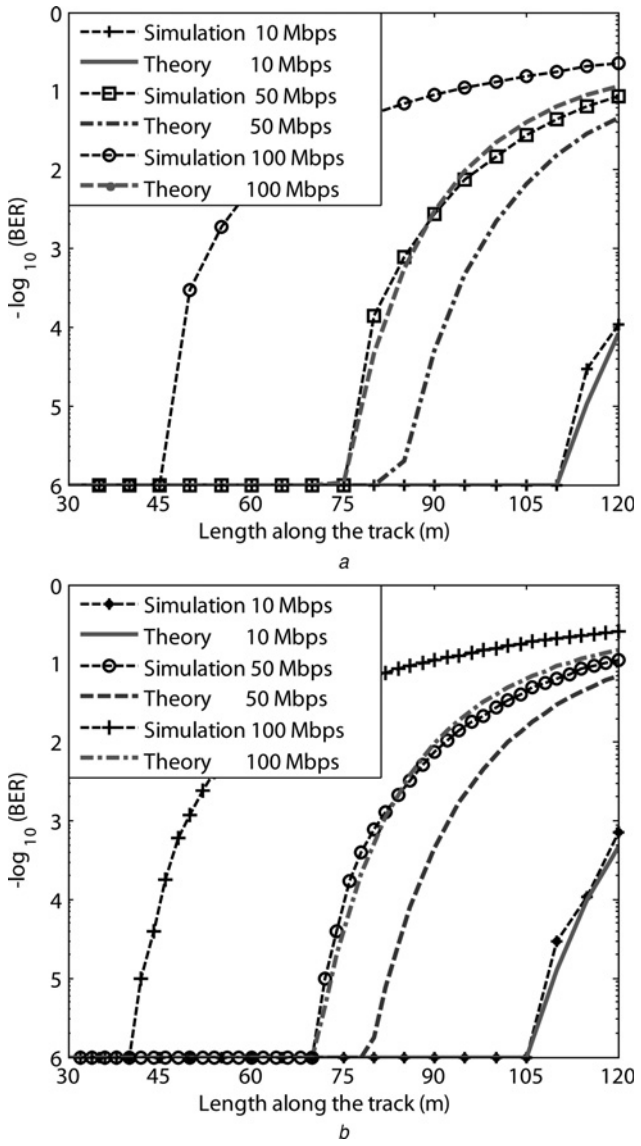

Fig. 9 *Bit error performance along the track for beam divergence*
a 3.2°
b 4°

typical value) is used to compare the achievable coverage length with the proposed beam angle. For an AWGN channel, the simulated BER curve shows a relatively good agreement with the predicted curve using (12) at 50 Mbps for both beam divergence angles, where 'good agreement' refers to variations $\leq 10\%$ between the two curves. For 100 Mbps case, there is mismatch between the predicted and the simulated results. This is because of the rise and fall times of the impulse response of the system, which is not ideal. The bandwidth of the laser limits the transmitted bit rate beyond 100 Mbps. The bit error performance of 10^{-6} is achieved for a track length of 75 m at 50 Mbps for a beam divergence of 3.2°. The coverage length drops to 68 m for a beam divergence of 4° for the same transmit power. For bit rates beyond 50 Mbps, the coverage length decreases for the desired BER because of the increase in the noise bandwidth of the system. The coverage length of 75 m with given beam divergence is to be used as a reference for the performance analysis of the system. However, moving to longer wavelengths could increase the transmitted power by up to 50 times, thereby increasing the effective coverage length along the track over few hundred metres. Thus, the number of BSs alongside the track could be significantly reduced. Hence, high bandwidth availability of FSO in excess of THz and license free operation [32] would encourage internet service providers to adopt this technology for ground-to-train communications.

5 Conclusions

A mathematical modelling for ground-to-train FSO communications link is proposed using Gaussian beam theory. Receiver power equation for a Gaussian source is derived based on the geometrical position of the BS from the track. The analytical and simulated BER performance of the proposed system is carried out showing a good agreement to each other for data rates up to 50 Mbps. With the optimum parameters, it is possible to have beam coverage for track length of 75 m for data rates up to 50 Mbps. Also, link budget analysis for the proposed system is presented showing a link margin of 17.75 dB for worse weather conditions. The paper also pointed out the proper positioning of the receiver on the train based on the aerodynamics of the train. Hence, FSO technology with the proposed system modelling can be an alternative to provide a high bandwidth broadband access to high speed trains.

6 Acknowledgment

R. Paudel thanks the Faculty of Engineering and Environment Northumbria University for financially supporting this research. This work was supported in part by the EU FP7 Cost Actions of IC0802 and IC1101.

7 References

1 Ciaramella, E., Arimoto, Y., Contestabile, G., *et al.*: '1.28 terabit/s (32 × 40 Gbit/s) wdm transmission system for free space optical communications', *IEEE J. Sel. Areas Commun.*, 2009, **27**, (9), pp. 1639–45
2 Henniger, H., Wilfert, O.: 'An introduction to free-space optical communications', *Radio Eng.*, 2010, **19**, (2), pp. 203–12
3 Wang, K., Nirmalathas, A., Lim, C., Skafidas, E.: 'Experimental demonstration of a full-duplex indoor optical wireless communication system', *IEEE Photonics Technol. Lett.*, 2012, **24**, (3), pp. 188–90
4 Langer, K.D., Grubor, J., Bouchet, O., *et al.*: 'Optical wireless communications for broadband access in home area networks'. Tenth Anniversary Int. Conf. on Transparent Optical Networks, 22–26 June 2008
5 Paraskevopoulos, A., Vučić, J., Voss, S.H., Swoboda, R., Langer, K.D.: 'Optical wireless communication systems in the Mb/s to Gb/s range, suitable for industrial applications', *IEEE/ASME Trans. Mechatronics*, 2010, **15**, (4), pp. 541–7
6 Le-Minh, H., O'Brien, D., Faulkner, G., *et al.*: 'A 1.25-Gb/s indoor cellular optical wireless communications demonstrator', *IEEE Photonics Technol. Lett.*, 2010, **22**, (21), pp. 1598–600
7 Wang, K., Nirmalathas, A., Lim, C., Skafidas, E.: 'High-speed optical wireless communication system for indoor applications', *IEEE Photonics Technol. Lett.*, 2011, **23**, (8), pp. 519–21
8 Cvijetic, N., Dayou, Q., Jianjun, Y., Yue-Kai, H., Ting, W.: '100 Gb/s per-channel free-space optical transmission with coherent detection and MIMO processing'. Thirty-fifth European Conf. on Optical Communication, 20–24 September 2009
9 Ahmad, I., Habibi, D.: 'A novel mobile WiMAX solution for higher throughput'. Sixteenth IEEE Int. Conf. on Networks, 12–14 December 2008
10 O'Brien, D.C., Katz, M., Wang, P., *et al.*: 'Short-range optical wireless communications' (Wireless World Research Forum, 2005)
11 Hiruta, M., Nakagawa, M., Haruyama, S., Ishikawa, S.: 'A study on optical wireless train communication system using mobile object tracking technique'. Eleventh Int. Conf. on Advanced Communication Technology, 15–18 February 2009

12 Haruyama, S., Urabe, H., Shogenji, T., *et al.*: 'New ground-to-train high-speed free-space optical communication system with fast handover mechanism'. Optical Fiber Communication Conf. and Exposition (OFC/NFOEC) and the National Fiber Optic Engineers Conf., 2011

13 Paudel, R., Ghassemlooy, Z., Le Minh, H., Rajbhandari, S., Leitgeb, E.: 'Lambertian source modelling of free space optical ground-to-train communications'. Eighth Int. Symp. on Communication Systems, Networks and Digital Signal Processing, Poznan, Poland, 18–20 July 2012

14 Railway Electrification: 25 kV a.c. Design on British Railways. 1988

15 Goldsmith, P.: 'Gaussian beam quasioptical propogation and applications' (Wiley-IEEE Press, 1998, 1st edn.)

16 Kahn, J.M., Barry, J.R.: 'Wireless infrared communications', *Proc. IEEE*, 1997, **85**, (2), pp. 265–98

17 O'Brien, D.C., Faulkner, G., Le Minh, H., *et al.*: 'Gigabit optical wireless for a Home Access Network'. Twentieth IEEE Int. Symp. Personal, Indoor and Mobile Radio Communications, 13–16 September 2009

18 Majumdar, A.K., Ricklin, J.C.: 'Free-space laser communications: principles and advances' (Springer, New York, 2008)

19 Manor, H., Arnon, S.: 'Performance of an optical wireless communication system as a function of wavelength', *Opt. Soc. Am.*, 2003, **42**, (21), pp. 4285–94

20 Hu, G.Y., Chen, C.Y., Chen, Z.Q.: 'Free-space optical communications using visible light', *J. Zhejiang Univ. Sci. A [online]*, 2007, **8**, (2), pp. 186–191, available at http://www.springerlink.com/content/c15p16727203432r/fulltext.pdf

21 Khalighi, M., Xu, F., Jaafar, Y., Bourennane, S.: 'Double-laser differential signaling for reducing the effect of background radiation in free-space optical systems', *IEEE/OSA J. Opt. Commun. Netw.*, 2011, **3**, (2), pp. 145–54

22 Safety of laser products- Part 1: Equipment classification and requirements: IEC 60825-1:2007

23 Leitgeb, E., Plank, T., Awan, M.S., *et al.*: 'Analysis and evaluation of optimum wavelengths for free-space optical transceivers'. Twelefth Int. Conf. on Transparent Optical Networks, 2010

24 Weichel, H.: 'Laser beam propagation in the atmosphere' (SPIE, Bellingham, 1990)

25 Kim, I.I., McArthur, B., Korevaar, E.: 'Comparison of laser beam propagation at 785 nm and 1550 nm in fog and haze for optical wireless communications'. SPIE Proc. Optical Wireless Communications III. 2001, vol. 4214, pp. 26–37

26 Bloom, S., Korevaar, E., Schuster, J., Willebrand, H.: 'Understanding the performance of free-space optics', *J. Opt. Netw.*, 2003, **2**, (6), pp. 178–200

27 Lee, H.S.: 'Assessment of potential aerodynamic effects on personnel and equipment in proximity to high-speed train operations'. Washington, DC U S Department of Transportation, Contract No.: DOT-VNTSC-FRA-98-3, 1999

28 Baker, C.: 'The flow around high speed trains', *J. Wind Eng. Ind. Aerodyn.*, 2010, **98**, pp. 277–98

29 Ray, S.: 'T-box harnesses wind-energy when trains move across the tracks', (2011), available at http://www.ecofriend.com/entry/t-box-harnesses-wind-energy-when-trains-move-across-the-tracks/

30 Deng, P., Yuan, X., Zeng, Y., Zhao, M., Luo, H.: 'Influence of wind speed on free space optical communication performance for Gaussian beam propagation through non Kolmogorov strong turbulence', *J. Phys.*, 2011, **276**, pp. 1–11

31 Andrews, L.C., Phillips, R.L.: 'Laser beam propagation through random media' (SPIE Press, Bellingham, 2005, 2nd edn.)

32 Ghassemlooy, Z., Popoola, W., Rajbhandari, S.: 'Optical wireless communications: system and channel modelling with Matlab®' (CRC Press, 2012)

doi: 10.1049/iet-opt.2012.0047